

# Experimental Investigation of Transient Hydrodynamic Forces of a Single-Blade Centrifugal Pump

N. SAVILIUS, F.-K. BENRA (SUPERVISOR)

Department of Turbomachinery

University of Duisburg-Essen

D-47057 Duisburg

GERMANY

*Abstract:* - In a single-blade centrifugal pump the interactions between impeller and casing generate an unbalanced pressure field, which changes during one impeller revolution. This transient pressure field effects strong transient hydrodynamic forces on the rotor. In the present paper the construction of a test stand to perform experimental investigations on transient hydrodynamic forces of a single-blade centrifugal pump is described. Furthermore it specifies the treatment of the measured signals. To measure these forces the single-blade pump was equipped with special mountings for the roller bearings. These mountings were provided with strain gauges. After a calibration of the system transient hydrodynamic forces were measured. Additional measurement systems for the rotating angel of the impeller, the volume flow rate and the pressure head of the pump were established. All data were recorded simultaneously by a computer system.

*Key-Words:* - single-blade centrifugal pump, unsteady flow, hydrodynamic forces, strain gauges, time-variant measurements

## 1 Introduction

In most applications for wastewater conveyance single-stage radial pumps are used. Wastewater often contains of fibrous and bulky compounds. This requires a special impeller geometry to prevent the pump from operational disturbance by clogging. Therefore the use of single-blade impellers got usual in the design of wastewater pumps. The single-blade design offers the largest flow channel cross-section. That allows fibers and solid compounds to pass the flow channel without clogging it. Another advantage is the possibility of thickening the leading edge of the blade without decreasing the cross section of the flow channel significantly. The durability of the leading edge against impact of solid compounds is enhanced and fibers are more likely slipping off the leading edge instead of laying around it.

But the single blade design brings additional problems during operation. As the field of flow does not properly follow the skeleton line of the blade and because of an interaction between rotor and stator, an unbalanced pressure field is generated. This causes a force acting on the impeller. That force is also indicated as hydrodynamic imbalance [1-4]. Additionally the pressure field changes during one impeller revolution because of the changing interaction between impeller and casing [5]. The result is a strong transient hydrodynamic force, which is periodic with the rotor turning, acting at the impeller and at the rotor shaft and setting the whole pumping set and equipment compounds in heavy vibrations. These vibrations often

lead to pump failure and to damages of the attached pipes.

As an example Fig.1 shows the vibration characteristics of the single-blade centrifugal pump investigated in this paper. In this case measurements have been done with vibration-velocity-sensors in two different radial directions. A periodicity with the rotor turning is obvious as one revolution lasts 0,04s at a turning frequency of 25Hz. The effective vibration velocity turns out to be 19mm/s in x-direction and 54mm/s in y-direction.

## 2 Problem Formulation

To realize deeper investigations on the hydrodynamic imbalance of single-blade radial pumps besides numerical simulation [5;6] a test stand has to be designed. It allows validating results taken from CFD and provides a view on the operating characteristics under real conditions.

A method for the measurement of hydrodynamic forces acting on the impeller in radial direction has to be developed. These forces have to be correlated to the rotating angle of the rotor. To achieve a satisfying resolution a number of about 1000 measurements per rotor revolution has to be recorded. As the rotor is turning with 25Hz this means a sampling rate of about 25000 samples per second for each signal. In addition to that the volume flow through the pump and the pressure head have to be measured to operate the pump at defined operating conditions.

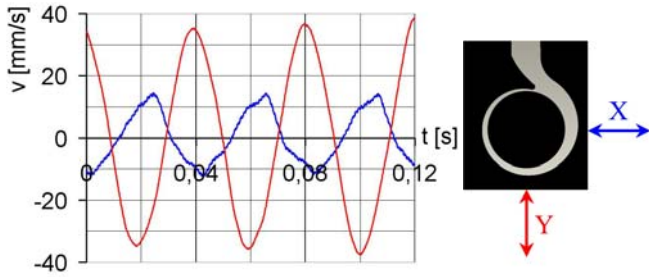


Fig.1 Vibration characteristics of the investigated single-blade centrifugal pump

### 3 Setting up the Test Stand

#### 3.1 General Layout

Fig.2 provides an overview of the test stand and shows the locations of the sensor equipment. The test stand consists of a basin, in which the pump is mounted upside down. The pump is driven via an ac motor over a belt pulley. The water is pumped into a duct, which directs it through a volume flow meter and a choke valve back into the tank. The flow is pacified as it passes through a reticule. Finally it enters the pump again.

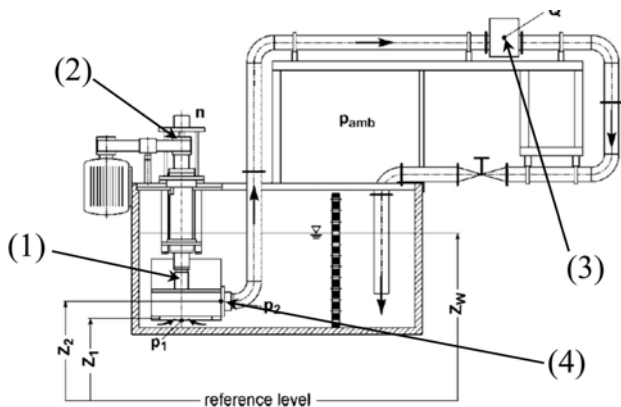


Fig.2 Overview sketch of the test stand

- (1) sensor-system for radial forces (sec. 3.2)
- (2) rotating angle sensors (sec. 3.4)
- (3) volume flow sensor (sec. 3.4)
- (4) pressure sensor (sec. 3.4)

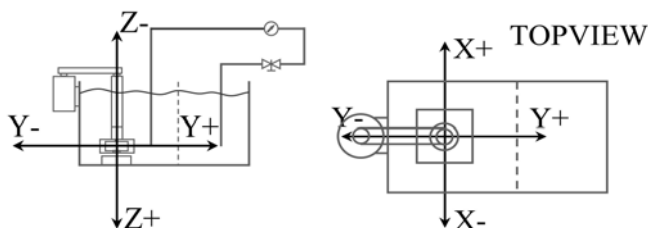


Fig.3 Definition of the coordinate system

In the following the cartesian coordinate system defined in Fig.3 will be used. The origin of this coordinate system is placed on the lower end of the drive shaft.

#### 3.2 Sensor System for Radial Forces

To measure radial forces special mountings for the fixed and the loose bearing of the lower drive shaft were designed. Each of these mountings respectively provides the connection between shaft and casing only through four deformation elements. The deformations of these elements are measured by strain gauges. The deformation elements are designed in a way that only elastic deformation will take place according to the expected radial forces. In Fig.4 the positions of the strain gauges on the mountings are shown.

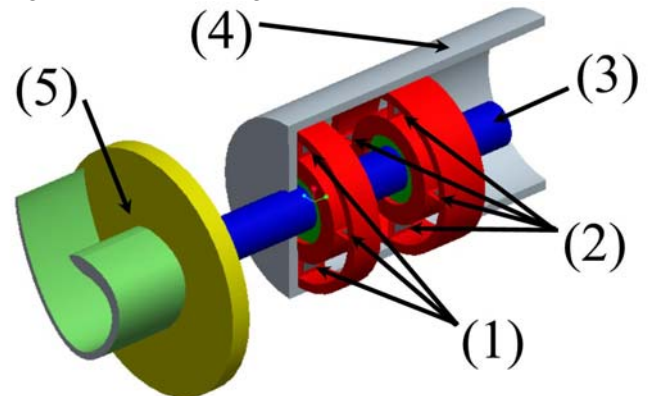


Fig.4 Positioning of strain gauges

- (1) Strain gauges at mounting for loose bearing
- (2) Strain gauges at mounting for fixed bearing
- (3) Cut rotor shaft
- (4) Cut housing
- (5) Impeller without shroud disk

To avoid the influence of a temperature change or bending of the deformation elements a Wheatstone full bridge of strain gauges is applied on all of the elements. So eight full bridges are established. In Fig.5 the configuration is exemplary shown for one element.

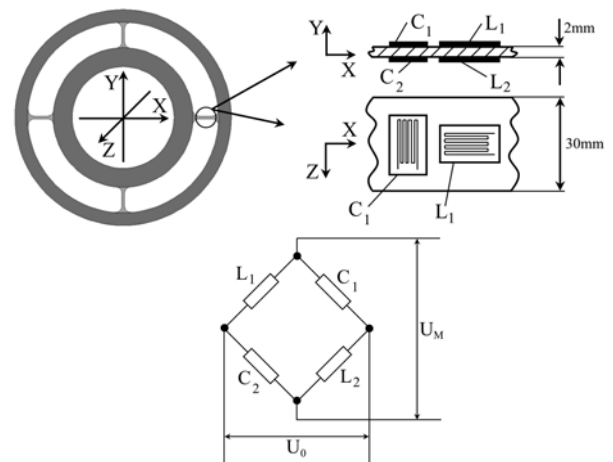


Fig.5 Configuration of Wheatstone full bridge

As all strain gauges have the same starting resistance  $R_0$  equation (1) describes the behavior of each full bridge by good approximation. And it explains the way of avoiding

the aforesaid influences. Equal changes  $\Delta R$  in all strain gauges by a change in temperature are eliminated in equation (1) and are taking no effect on the measured voltage  $U_M$ . In addition contrary changes of  $\Delta R$  in opposing strain gauges are eliminated too. This effect prevents influence by bending of the deformation elements.

$$U_M \approx \frac{U_0}{4R_0} (\Delta L_1 - \Delta C_1 + \Delta L_2 - \Delta C_2) \quad (1)$$

As the value of  $U_M$  is very small due to the small changes of the resistances it has to be enlarged by a measuring amplifier by a factor of 2000.

### 3.3 Calibration

For proper results an adequate calibration of the sensor system is necessary. For this reason the drive shaft of the pump is brought into horizontal position. Impeller and pump casing are removed. A defined mass is attached at the end of the drive shaft, which is the origin of the defined coordinate system. The reactions of the eight full bridges are amplified and recorded while the appended mass is increased stepwise. This procedure is repeated for eight positions of the housing of the bearings, which is turned stepwise about  $45^\circ$  to ensure that the system is working adequately in every direction. Fig.6 illustrates the procedure while one mounting represents the casing. For every measurement the signals are totalized as shown in equations (2) and (3). The nomenclature of the measured signals is related to the coordinate axes the particular full bridges are applicationed on. The result is one summed signal for each of the bearings for each of the eight casing positions.

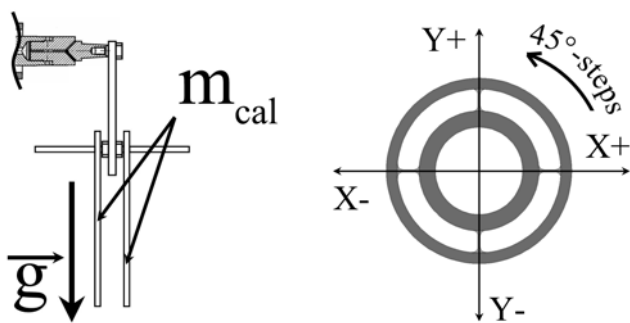


Fig.6 Build up for calibration

$$U_{tot\_fix} = \sqrt{(X_{fix,+} - X_{fix,-})^2 + (Y_{fix,+} - Y_{fix,-})^2} \quad (2)$$

$$U_{tot\_loo} = \sqrt{(X_{loo,+} - X_{loo,-})^2 + (Y_{loo,+} - Y_{loo,-})^2} \quad (3)$$

As the system is reacting the same way in each of the eight positions in sufficient approximation the average value over all positions is calculated for each calibration mass. The result is presented in Fig.7. The totalized

signals are correlated to the attached force, which can be determined by equation (4), as mass and gravitational constant are known.

$$F_g = m_{cal} * g \quad (4)$$

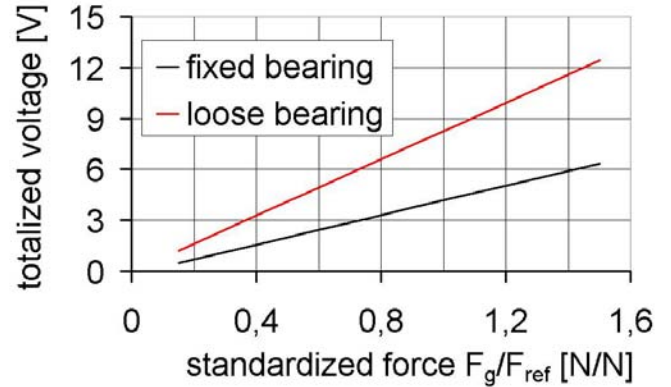


Fig.7 Calibration results

The calibration results in one calibration function for each bearing. One function suffices to calculate the acting force during forthcoming measurements. The second one is to check reliability. Equations (5) and (6) present the used calibration functions.

$$\frac{F_{fixed}}{F_{ref}} = 0,2306 \left[ \frac{1}{V} \right] * U_{sum\_fixe} [V] \quad (5)$$

$$\frac{F_{loose}}{F_{ref}} = 0,1206 \left[ \frac{1}{V} \right] * U_{sum\_loo} [V] \quad (6)$$

The procedure of calibration shows that the forthcoming measurements will evaluate the hydrodynamic forces in an approximated way. There are different reasons for this. On the one hand the acting point of the radial force on the impeller cannot be determined. The measurement will deliver radial forces acting at the end of the drive shaft, which are equivalent to the radial hydrodynamic forces on the impeller. But the hydrodynamic force itself and its acting point cannot be accessed. On the other hand there will be an influence generated by eccentric axial force acting on the impeller. Its momentum will take effect on the sensor system. Even if the axial force was measured the influence could not be determined because the acting point is unknown.

### 3.4 Additional Sensors

The forces have to be correlated to the blade position. Therefore two inductive sensors are used. Both are positioned at the belt pulley (sec. 3.1). The belt pulley provides a direct connection to the impeller. Fig.8 shows where the sensors are located at the belt pulley. Sensor

$S_0$  sends one signal per revolution. It interacts with one small cube of metal attached on top of the pulley. Sensor  $S_{36}$  sends 36 signals per revolution, as it interacts with the 36 teeth, which drive the belt. The sensors have a switching frequency of 3kHz. In operation the frequency of  $S_0$  will be about 25Hz and the frequency of  $S_{36}$  will be about 0.9kHz. So the switching frequency of the sensors is sufficient for this task.

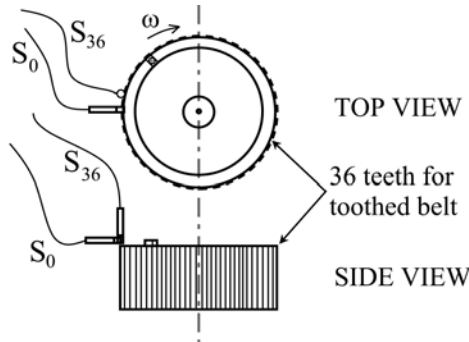


Fig.8 Inductive sensor positions at belt pulley

For the measurement of the volume flow a magnetic-inductive sensor is used. In this kind of sensor no mechanic solid parts are necessary in the flow. In this way it is possible to measure the volume flow without disturbing it.

A pressure transducer is used to determine the pressure at the outlet of the pump. The sensor is connected to a circular manifold, which is attached to the outlet via four drillings in 90°-steps. The sensor is supplied with 24V and gives out 4-20mA. This range of current is equivalent to a range of 0-4bar. The correlation is linear. Fig.9 shows a scheme of the whole measurement system and signal flow.

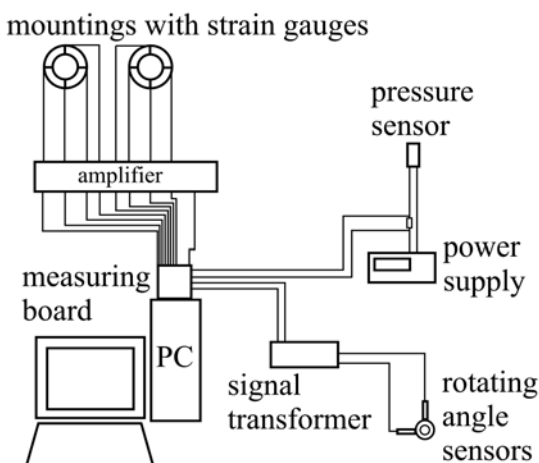


Fig.9 Measurement system

## 4 Results

### 4.1 Calculating Hydrodynamic Forces

Measurements have been done for four operating points. In addition to the design point of 146.16m<sup>3</sup>/h the volume

flows of 73.08m<sup>3</sup>/h (50%), 109.62m<sup>3</sup>/h (75%) and 164.02m<sup>3</sup>/h (maximum flow 112%) were investigated.

Each measurement lasted for 2.4 seconds. To achieve a proper resolution the sampling rate was set to 25kHz. In this way 60000 samples were taken from each of the eight full bridges and the two rotation angle sensors. In addition to that the signals were correlated to time. So altogether 660000 samples were taken per measurement. As the turning frequency of the impeller is 25Hz, about 1000 samples per rotation were measured, as demanded in the Problem Formulation.

To evaluate the data the signals of all measured rotations have to be averaged to a single rotation. Small variances in the measurements are compensated this way. As the amount of data is very high a special macro was programmed to do this work. The signals of sensor  $S_0$  are used as the starting point of each rotation.

In the next step the signals of the X- and the Y-axis are combined like it was done for the calibration but without calculating the absolute value. This is done for the loose and the fixed bearing to check the results.

$$U_{sum\_X} [V] = X_+ [V] - X_- [V] \quad (7)$$

$$U_{sum\_Y} [V] = Y_+ [V] - Y_- [V] \quad (8)$$

After the signals are combined the calibration function for the particular bearing is used to calculate the forces (sec 3.3). The result is one force in X- and one in Y-direction for each bearing. The results have to be the same for the loose and the fixed bearing.

To take a look at the absolute values of the forces they are combined and divided by a reference force (see equation (9)).

$$\frac{F_{rad}}{F_{ref}} \left[ \frac{N}{N} \right] = \sqrt{\left( \frac{F_x}{F_{ref}} \left[ \frac{N}{N} \right] \right)^2 + \left( \frac{F_y}{F_{ref}} \left[ \frac{N}{N} \right] \right)^2} \quad (9)$$

The signals of sensor  $S_{36}$  proved that the rotating velocity is constant during one revolution. Therefore the correlation between time and rotating angle is linear. So the measured forces can easily be displayed correlated to the actual impeller position. The signal of sensor  $S_0$  is used as the 0°-position of the impeller. Fig.10 shows the impeller position for some rotating angles  $\phi$ . In addition the symbols, which will be used in Fig.12, are displayed.

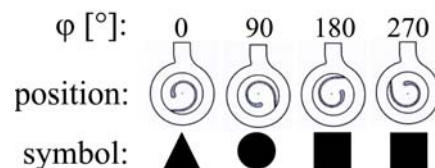


Fig.10 Impeller position and rotating angle

### 4.2 Hydrodynamic Forces

Fig.11 shows the absolute values of the radial forces plotted versus the impeller position. These absolute values are calculated with equation (9). The lines can be divided into two characteristic shapes. The lines of the two lower volume flows look alike. So do the lines of the higher volume flows. The variances of the forces and the absolute maximums are higher for the lower volume flows. The lines of the higher volume flows are smoother but the average values are higher.

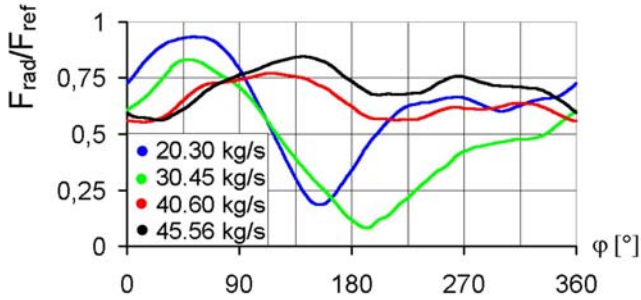


Fig.11 Absolute values of radial forces

Fig.12 provides a view on the radial forces in the absolute coordinate system. To provide a correlation to the actual blade position, the symbols introduced in Fig.10 are used. The dimensions of the orbits in the absolute system are increasing with the volume flow. This leads to the first conclusion. The hydrodynamic imbalance is dependent on the volume flow. For this reason it can also be correlated to the pressure head because the pressure head is dependent on the volume flow.

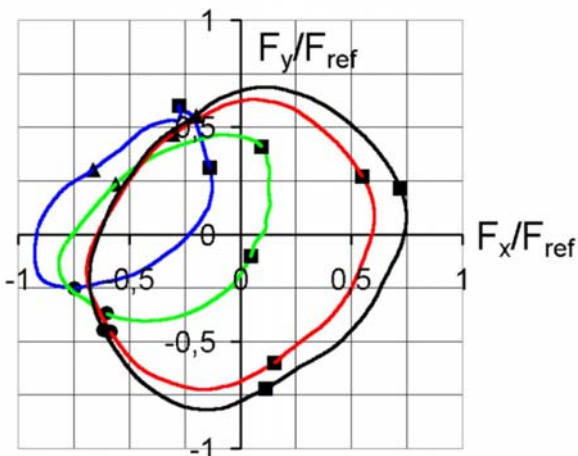


Fig.12 Orbit of radial forces in the absolute system

To take a closer look at the imbalances Fig.13 and Fig.14 present the hydrodynamic forces separated in X- and Y-direction. The aforesaid tendency of an increasing of the hydrodynamic forces as a function of the volume flow becomes more obvious here. Not only the average values but also the amplitudes of the forces are rising.

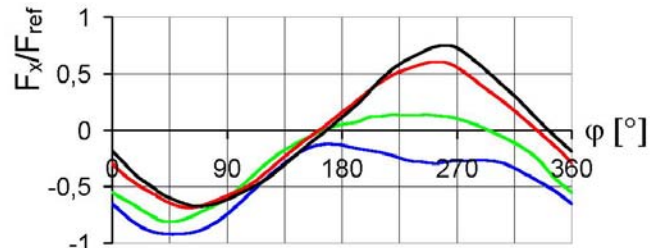


Fig.13 Hydrodynamic forces in X-direction

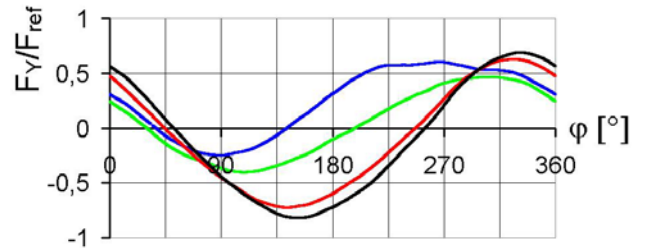


Fig.14 Hydrodynamic forces in Y-direction

In the following some characteristics of the hydrodynamic imbalance will be formulated and investigated to bring all information together.

One significant characteristic is the amplitude of the hydrodynamic imbalance as it generates danger of operational disturbances. A constant force would harm the bearings but it would not generate vibrations, which could harm the whole pumping set. Because of this a closer look at the amplitudes in X- and Y-direction (see Fig.13;14) correlated to the volume flow is taken. In addition the average value of the absolute force values (see Fig.11) is analyzed and correlated to the volume flow as it provides information of the average forces harming the bearings. In Fig.15 the results of this analysis are presented.

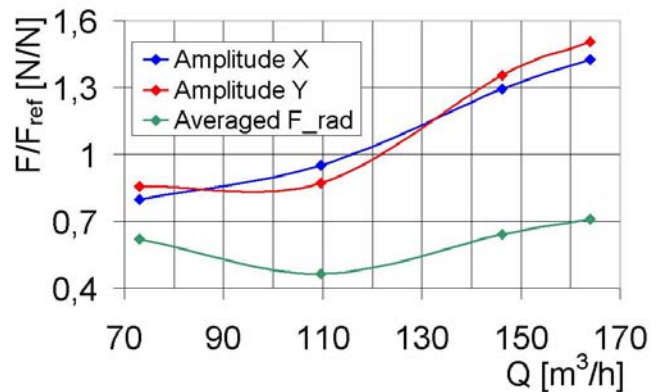


Fig.15 Analysis of amplitudes and average values

If the values below a volume flow of  $110m^3/h$  are disregarded, the curves are nearly linear. This disregard is justifiable because the lower volume flow is far away from the design point of the pump, which is  $146,16m^3/h$ . So it will not be common during operation. Equations (10), (11) and (12) are the results of the linearizations.

$$\frac{Amp_X}{F_{ref}} \left[ \frac{N}{N} \right] = 0,0088 \left[ \frac{N \cdot h}{N \cdot m^3} \right] * Q \left[ \frac{m^3}{h} \right] - 0,0119 \left[ \frac{N}{N} \right] \quad (10)$$

$$\frac{Amp_Y}{F_{ref}} \left[ \frac{N}{N} \right] = 0,0119 \left[ \frac{N \cdot h}{N \cdot m^3} \right] * Q \left[ \frac{m^3}{h} \right] - 0,4215 \left[ \frac{N}{N} \right] \quad (11)$$

$$\frac{AveF_{rad}}{F_{ref}} \left[ \frac{N}{N} \right] = 0,0045 \left[ \frac{N \cdot h}{N \cdot m^3} \right] * Q \left[ \frac{m^3}{h} \right] - 0,0291 \left[ \frac{N}{N} \right] \quad (12)$$

loo at loose bearing  
rad in radial direction  
ref reference  
sum summed  
tot totalized  
X x-direction  
Y y-direction  
+ positive coordinate axis  
- negative coordinate axis

Now these functions can be use to interpolate values for operating points between 110m<sup>3</sup>/h and 164m<sup>3</sup>/h.

## 5 Conclusion

It was managed to measure transient hydrodynamic forces of a single-blade centrifugal pump. Furthermore it was possible to gain linear functions describing the hydrodynamic imbalance as a function of volume flow for the investigated pump. In general an increasing of the volume flow affects a rise of the hydrodynamic imbalance.

The technique of using strain gauges was a success. The test stand can be used to manage further investigations on single-blade or other centrifugal pumps as impeller and casing can be exchanged easily.

The applied technique of using strain gauges can be transferred to any other rotating machinery to measure forces on the rotor.

## 6 Nomenclature

C	Ω	resistance of cross strain gauge
g	m/s <sup>2</sup>	gravitational constant
F	N	force
F <sub>G</sub>	N	gravitational force
L	Ω	resistance of longitudinal strain gauge
m <sub>cal</sub>	kg	calibration mass
Q	m <sup>3</sup> /h	volume flow
R <sub>0</sub>	Ω	strain gauge resistance
t	s	time
v	mm/s	velocity
U	V	voltage
U <sub>0</sub>	V	supply voltage
U <sub>M</sub>	V	measured voltage
X	V	full bridge signal
Y	V	full bridge signal
Δ	--	difference
φ	°	rotating angle

## Subscripts

cal	calibration
fix	at fixed bearing

## References:

- [1] Agostinelli, A.; Nobles, D.; Mockridge, C. R. (1960), An Experimental Investigation of Radial Thrust in Centrifugal Pumps, *Transactions of the ASME, Journal of Engineering for Power*, Vol. 82, No. 2
- [2] Okamura, T. (1980), Radial Thrust in Centrifugal Pumps with a Single-Vane-Impeller, *Bulletin of the JSME* 23, No. 180
- [3] Aoki, M. (1984), Instantaneous Interblade Pressure Distributions and Fluctuating Radial Thrust in a Single-Blade Centrifugal Pump, *Bulletin of the JSME* 27, No. 233
- [4] Gülich, J.; Jud, W.; Hughes, S. F. (1987), Review of Parameters Influencing Hydraulic Forces on Centrifugal Impellers, *Proc. Inst. Mech. Engineers*, Vol. 201, No. A3
- [5] Benra, F. K.; Dohmen, H. J.; Schneider, O. (2003), Unsteady Flow in Single-Blade Sewage Water Pumps, *2nd International Conference on Heat Transfer, Fluid Mechanics and Thermodynamics*, Paper No. BF1
- [6] Benra, F. K.; Sommer, M.; Müller, M.; Töws, A. (2004), Investigation of the Three-Dimensional Time Accurate Flow in Single-Blade Sewage Water Pumps, *Proceedings of the Fourth South African Conference of Applied Mechanics, SACAM'04*